View Article Online / Journal Homepage / Table of Contents for this issue
Dynamic Article Links

PCCP

Cite this: *Phys. Chem. Chem. Phys.*, 2011, **13**, 12826–12834

www.rsc.org/pccp

PAPER

Comparison of a calculated and measured XANES spectrum of α-Fe_2O_3

Pieremanuele Canepa, Eleanor Schofield, Alan V. Chadwick and Maria Alfredsson*

Received 5th January 2011, Accepted 23rd May 2011
DOI: 10.1039/c1cp00034a

Comparison and prediction of the experimental XANES spectrum is a good measurement of the quality of the electronic structure calculations employed, and their ability to predict electronic transitions in solids. Here we present a comparison between BLYP + *U* and hybrid-BLYP calculations regarding the geometric, magnetic and electronic structures of α-Fe_2O_3 (hematite). Several values of *U* and different percentages of Fock-exchange have been screened to see how their contributions affect different properties of hematite, paying particular attention to the electronic structure. To estimate the quality of the various methods the calculated density-of-states were compared to the experimentally collected XANES spectrum of the iron K-edge, providing information about the orbitals describing the conduction band. We find that in agreement with previous studies DFT + *U* and hybrid-functional simulations can correctly predict the character of the valence band, but only Fock-exchange higher than 30% or *U*-values equal or larger than 6 eV properly reproduce the order between the t_g and e orbitals in the conduction band, and can, therefore, be used to study and predict XANES spectra and electronic transitions in hematite.

Published on 15 June 2011. Downloaded by National University of Singapore on 12/2/2018 5:54:21 AM.

A. Introduction

In recent decades, the theory of functional density (DFT) has been successfully employed in predicting structures and properties of most bulk materials.[1,2] However, DFT fails to do so for strongly correlated systems, such as NiO,[3–8] MnO,[4,5,9] FeO[4,5,10] and CoO.[4,5,8] These systems are predicted with DFT as metallic, but experimentally described as Mott insulators. This is because of the strong correlation, arising from the on-site Coulomb repulsion, between the d-electrons on the transition metal sites. As a matter of fact the resulting (DFT) charge density remains largely delocalised, not accounting correctly for the strong correlation effects. The most widely used theories to overcome this problem are the Hubbard *U* correction (DFT + *U*) and hybrid-functionals.

Another class of strongly correlated materials is that of the charge-transfer insulators. These materials are often described by pure DFT simulations as Mott insulators (see *e.g.* ref. 11–14), and, therefore, showing a band gap in the solids, but wrongly associating the highest occupied eigenvalues in the valence band (VB) with the d-electrons on the transition metal. This observation is, as for the Mott-insulators, linked with the high delocalisation of the d-electrons on the transition metal site, and may be corrected for by employing the DFT + *U* or hybrid-functional simulations.[4,6,7,9,10,15,16]

School of Physical Sciences, Ingram building, University of Kent, Canterbury CT2 7NH, UK. E-mail: m.l.alfredsson@kent.ac.uk; Fax: +44 (0)1227 827558; Tel: +44 (0)01227 823237

α-Fe_2O_3 (also referred to as hematite) has experimentally been described as an insulator with charge-transfer character belonging to the latter category.[13,17] As expected, DFT describes hematite as a Mott insulator with an energy band gap of *ca.* 0.5 eV, which is too small when compared to that measured experimentally (*ca.* 2 eV).[12,13,17–19] Models using DFT + *U* or hybrid-functionals accurately predict hematite as a charge-transfer insulator. Both techniques successfully describe the valence band of hematite localising the d-electrons on the iron-sites. The result is that the top of the VB is experimentally[20–22] and theoretically[12,13,17–19,23] identified as oxygen sp-electrons, which agrees with the definition of a charge-transfer insulator.

Thus, an accurate description of the VB relies on the *U* value or the percentage of Hartree–Fock exchange chosen in the calculations. This is also true for the conduction band (CB). To gain information about the character of the conduction band experimental techniques such as X-ray photoelectron spectroscopy (XPS) or ultraviolet photo-emission spectroscopy (UPS) may be employed. Such measurements suggest that the lowest unoccupied states in the CB are characterised by Fe d-electrons, which again agrees with the definition of a charge-transfer insulator. Theoretically, both DFT + *U* ($U \leq 4$)[13,18,24] and B3LYP[12] (20% Hartree–Fock exchange) correctly predict this behaviour.

However, UPS and XPS do not give the orbital symmetry, which instead can be interpreted experimentally from the pre-edge of X-ray absorption near-edge structure (XANES) or resonant inelastic X-ray scattering (RIXS) measurements.

 This journal is © the Owner Societies 2011

View Article Online

Published on 15 June 2011. Downloaded by National University of Singapore on 12/2/2018 5:54:21 AM.

Using a single electron excitation model the interpretation of the pre-edge XANES spectra of hematite is consistent with a quadrupole transition of a 1s core electron to the empty 3d states.[24] In addition, for materials such as α-Fe_2O_3 that lacks inversion symmetry also dipole transitions need to be considered. For materials with dipole transitions the symmetry of the d orbitals can be determined by identifying the intensity ratios between the t_g and e in the pre-edge (XANES, RIXS) spectrum. Proposing that for hematite the e has higher intensity than the t_g orbitals, and is shifted to slightly higher energy values. The latter interpretation is consistent with crystal field theory, for which the t_g orbitals are expected to be lower in energy (more stabilised) than the e orbitals. Hence, a comparison between the experimentally obtained pre-edge XANES on the Fe K-edge and the total density of state (DOS) obtained with DFT + U and hybrid-functionals can be used to reproduce and predict XANES spectra. For hematite DFT + U ($U \leq 4$) and B3LYP calculations seem to fail in the prediction introduced above, over stabilising the e orbitals compared to the t_g ones. This behaviour has previously also been pointed out by Glatzel *et al.*[24]

It is well known that electron excitations in charge-transfer solids and molecules are difficult to reproduce by DFT + U[5,24] and hybrid-functionals, but also by time-dependent DFT (TD-DFT) simulations.[8,25–32] The problem is associated with long-range self-interactions. Recently new functionals have been described in the literature to correct for this inaccuracy, but appear to have the effect of solely lowering the band gap, without altering the ordering of the eigenvalues as shown by, for example, Scuseria and co-workers.[7,33–35]

Considering that hematite is relevant in many technological applications such as energy storage materials[36–38] and catalysis,[39–41] for which chemical reactions and transitions are of importance, it is vital that first principles calculations reproduce hematite as accurate as possible. In addition, hematite is one of the most common minerals, and researched for its environmental applications. It is for example used to immobilise contaminants like heavy metals in soils.[21,42–47]

The aim of this study is to find a computer model, allowing us to correctly predict the electronic structure of α-Fe_2O_3, by comparing DFT + U and hybrid-functionals with experimentally recorded XANES data on the Fe K-edge in hematite. An accurate description of the valence and conduction bands imposes that we will be able to study electron transitions (and chemical reactions) in charge-transfer insulators, of which hematite is one material. In fact, the wrong prediction of the orbital symmetry order would wrongly affect well-established electronic phenomena such as σ- and π-back-donation when molecules like CO or NO are adsorbed on hematite. For example, the correct description of the π-back-donation is important when CO is adsorbed on sulfur-contaminated α-Fe_2O_3 as observed by Magnacca *et al.*[48] Furthermore, XAFS measurements revealed that the de-hydrogenation of ethyl-benzene and styrene on hematite surfaces is eventually determined by their adsorption geometries on the surface, which maximizes the π-back-donation between the acid iron-sites and the relevant molecular orbitals.[49] Important is also the role played by the lower-lying exited states in α-Fe_2O_3 in the photodissociation of water for hydrogen production.[50–53] The correct description of the conduction band would also allow us to predict, using a one-electron Hamiltonian, the XANES spectra, which is attractive owing to its low computational cost compared to multi-configuration methods.

By comparing an experimentally recorded XANES spectrum and first principles calculations, we show that only by employing U-values larger or equal to 6 eV or higher than 30% of Hartree–Fock exchange we can predict the appropriate order of the t_g and e d-orbitals in the conduction band of hematite. Other properties are less method dependent.

B. Computational and experimental details

2.1 Computational

All geometry optimizations have been done starting from the X-ray data of the rhombohedral α-Fe_2O_3 structure ($R\bar{3}c$) presented in Fig. 1 and Table 1.[54]

In Fig. 1 sFe–Fe describes the distance between the Fe1 and Fe2 (or Fe3 and Fe4) ions, whereas lFe–Fe indicates the longer Fe–Fe distance between the Fe2 and Fe3 sites.

An anti-ferromagnetic order, + − − + (see Fig. 1) where the spin configurations on the iron atoms are Fe1 ↑, Fe2 ↓, Fe3 ↓ and Fe4 ↑, was imposed in all calculations. This spin-configuration was found to be the energetically most favorable one when compared to alternative magnetic orders, and in agreement with previous simulations.[13,17,18] All simulations have been spin corrected.

The calculations have been carried out with the PWscf (from the 'QUANTUM ESPRESSO' package) and the CRYSTAL06 codes.[55,56] Though both codes can employ density functional theory, CRYSTAL06 can also use the Hartree–Fock (HF) approach, allowing us to design

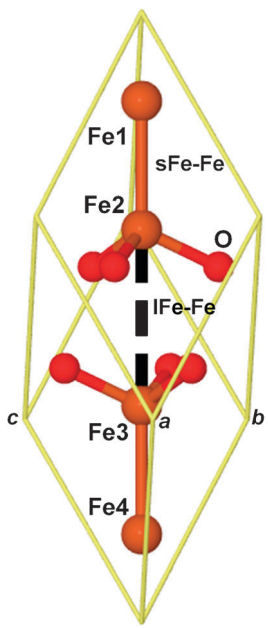

Fig. 1 Bulk structure of α-Fe_2O_3 in the rhombohedral space group $R\bar{3}C$.[22] sFe–Fe indicates the distance between the Fe1 and Fe2 (or Fe3 and Fe4) ions, whereas lFe–Fe describes the distance between Fe2 and Fe3. This picture has been made using J-ICE.

View Article Online

Published on 15 June 2011. Downloaded by National University of Singapore on 12/2/2018 5:54:21 AM.

Table 1 Lattice parameters (a) and bond lengths (sFe–Fe, lFe–Fe and Fe–O) for α-Fe_2O_3 are expressed in Å, volume of the cell (V) and angle (α) in Å^3 and degrees, respectively. U is in eV. Func. states functional. Numbers in brackets represent values obtained (with the same Hamiltonian description) by using the ECP for describing both Fe and O electrons rather than an all-electron basis-set

Models								
PW	Func.	U	a	α	V	sFe–Fe	lFe–Fe	Fe–O
	PBE	0.00	5.46	54.79	101.13	2.943	3.995	1.932
	BLYP	0.00	5.53	54.68	104.55	2.996	4.031	1.947
	BLYP	1.00	5.54	54.82	105.71	2.995	4.043	1.959
	BLYP	2.00	5.55	54.95	106.71	2.986	4.061	1.971
	BLYP	3.00	5.56	55.07	107.60	2.971	4.082	1.985
	BLYP	3.75	5.57	55.16	108.44	2.958	4.102	1.997
	BLYP	4.00	5.57	55.20	108.63	2.957	4.104	1.999
	BLYP	5.00	5.58	55.31	109.65	2.945	4.125	2.013
	BLYP	6.00	5.60	55.40	110.66	2.932	4.015	2.026
Ref. 13	PW91	0.00	—	—	—	2.941	4.006	—
Ref. 18	PBE	0.00	5.48	54.70	101.46	2.947	4.002	1.934
Ref. 18	PBE	3.30	5.50	55.19	104.49	2.929	4.044	1.972
LCAO	Func.	HF%						
	PBE	0	5.44	55.07	101.07	2.953	3.955	1.934
	BLYP	0	5.49 (5.52)	54.89 (54.85)	103.13 (104.99)	2.982 (2.990)	3.993 (4.025)	1.943 (1.952)
	F10LYP	10	5.49	55.11	103.67	2.984	3.998	1.950
	B3LYP	20	5.47	55.27	103.04	2.963	3.968	1.953
	F30LYP	30	5.45	55.37	102.24	2.942	3.958	1.952
	F40LYP	40	5.43 (5.44)	55.47 (55.45)	101.50 (102.03)	2.922 (2.900)	3.951 (3.986)	1.951 (1.946)
	F50LYP	50	5.42	55.54	100.77	2.907	3.942	1.950
	HF[a]	100	5.46	55.69	103.60	2.803	4.000	1.975
Ref. 17	HF[b]	100	5.47	55.70	104.18	2.877	—	1.988
Ref. 12	B3LYP	20	5.49	55.06	103.56	2.998	—	2.142
Exp.[22]	—	—	5.43	55.28	100.62	2.896	3.977	1.945

[a] A smaller all-electron basis-set than that in the present paper was used. [b] These data were carried out with the Durand ECP.

hybrid-functionals by combining various amount of HF and DFT exchange with suitable correlation functionals. PWscf instead provides the Hubbard U (DFT + U) correction.[15,16]

2.1.1 Plane-wave simulations—DFT + *U*. In the PWscf code the description of the cores for the iron and oxygen atoms was done adopting ultrasoft Vanderbilt pseudo-potentials.[57] These pseudo-potentials also take into account scalar relativistic effects. The remaining valence electrons, ten for each iron atom and six for each oxygen atom, were represented by plane-waves (PW) with an optimized cutoff of 680 eV. In all calculations we used the Becke Lee–Yang–Parr (BLYP) or Perdew–Burke–Ernzerhof (PBE) pseudo-potentials along with their corresponding functionals.[58–60] We employed a k-point mesh of 4 × 4 × 4. With these settings the difference in the total energy with respect to a simulation using a 6 × 6 × 6 k-point grid along with a cutoff of 816 eV is less than 0.01 eV per atom.

Ionic positions and cell parameters were optimized with the Broyden Fletcher Goldfarb Shanno (BFGS) algorithm.[61–64]

To ensure a good convergence of the self-consistent field (SCF) cycles the tolerance on the energy was fixed to 1×10^{-7} eV, whereas all the remaining tolerance values, including those involved in the geometry optimization, were kept as the default ones.

To study strongly correlated systems Anisimov and coworkers developed a first principles strategy, DFT + U.[65] Here, we applied the BLYP + U method to α-Fe_2O_3, following two distinct approaches:

1. We varied the U-value between 1 and 6 eV. For each U-value the structure was optimized, aiming to understand the dependence of some properties when U is varied.

2. We derived self-consistently a suitable value of U, using the linear response theory adapted for the PWscf code by Cococcioni *et al.*[15,16] Then, by using the obtained U-value, we optimized the structure for comparison with approach 1.

The latter approach consists in running a few single energy points of a supercell of α-Fe_2O_3, in which the electronic occupation of one isolated iron atom is varied by shifting a localized electric field. The previous literature has suggested employing either the 2 × 2 × 1 or the 2 × 2 × 2 supercell for hematite, whilst the electric field applied ranges between −0.2 and 0.2 eV.[18] We found an optimized value of U of 3.75 ± 0.05 eV using a 2 × 2 × 2 supercell along with the proposed field range.[18]

The U-value obtained is in good agreement with what has been previously optimized by Blanchard *et al.* (3.3 eV), using the PBE functional and its corresponding pseudo-potentials, although considering eight valence electrons on the Fe atoms.[18] Our value also agrees with the U-value used by Rollmann *et al.* of 4 eV, which was optimized by fitting the band gap to the experimental value.[13]

2.1.2 Linear combination of crystalline orbitals (LCAO)—hybrid functionals. The multi-electron wave function in CRYSTAL06 is defined as a linear combination of crystalline orbitals (LCAO), which are expanded in terms of Gaussian-type basis sets. For iron a 86-411d41G*[17] and for oxygen a 8-411G[66] basis set were chosen. However, to make our LCAO data more comparable with the PW results we also used for both iron and oxygen a small-core effective pseudopotential (ECP).[67–69] The valence electrons not accounted by the ECP are described for oxygen (3-21G) and iron (4-211G*) basis sets, respectively.

 This journal is © the Owner Societies 2011

View Article Online

Published on 15 June 2011. Downloaded by National University of Singapore on 12/2/2018 5:54:21 AM.

The most commonly used hybrid-functional in the literature is the B3LYP one. In B3LYP, 20% of HF exchange is mixed with 80% of Becke exchange, in combination with the LYP correlation functional.[58,59] This combination has been proven successful to model molecular systems.[70] However, previous studies show that 20% HF exchange is not always satisfactory for modelling solids.[7,10,71]

Hence, to compare the B3LYP functional with hybrids using a higher contribution of HF exchange we have chosen to work with hybrid-BLYP functionals.

The CRYSTAL06 calculations were performed with the BLYP, PBE and hybrid-BLYP functionals using 10 to 50 percentage of HF exchange.[72] These functionals are denoted FXLYP, where X indicates the amount of HF exchange.

Since in CRYSTAL06, the exchange–correlation contribution is carried out by a numerical integration of the electron density over set grid points, a pruned grid of 75 radial points has been chosen along with one sub-interval with 974 angular points. The irreducible Brillouin zone (IBZ) was sampled using a $6 \times 6 \times 6$ k-point grid.

A complete relaxation of both ionic coordinates and cell parameters of α-Fe_2O_3 was carried out by means of the BFGS algorithm (as adopted within the PW calculations, see Section 2.1).

The remaining parameters such as thresholds for the integral selection, the integrated density, the maximum forces, and the maximum atomic displacements were chosen as the default values.

2.2 Experiment—XANES

The α-Fe_2O_3 XANES (X-ray absorption near-edge structure) spectra were recorded on the SAMBA beamline, a station located on a bending magnet at the SOLEIL (GIF-sur-YVETTE, Paris) synchrotron (operating at 300 mA, 2.75 GeV, top up mode). Spectra were collected in transmission mode at the Fe K-edge with a sagittal focusing double crystal Si(220) and focusing mirrors graded at 5 mrad to remove the harmonics. The beam spot was de-focused to reduce the photon flux and prevent beam damage to the sample. The XANES spectra were normalized using SIXPACK.[73]

C. Results

In this section we compare, first of all, the geometric and magnetic structure of the solid obtained with the BLYP + U and hybrid-BLYP functionals. It is our experience that wrongly reproduced geometric properties are often a result of a poor description of the electronic structure.[11] Hence a good starting point is to reproduce the geometric properties as well as possible. Secondly, the electronic properties of α-Fe_2O_3 will be discussed in comparison with XANES data.

3.1 Geometric structure

Cell parameters, bond lengths and volumes of the fully optimized structure of rhombohedral α-Fe_2O_3, are presented in Table 1.

For comparison with previous simulations and for justification of our choice of pseudopotentials and basis sets we start by presenting results for the pure DFT calculations. It is found that BLYP lattice parameters and bond lengths match with those obtained with the PBE functional, and also with the literature regarding PW91 data.[13] This is an important observation for the PW calculations, as the pseudo-potentials used in the two simulations are slightly different. The same basis-sets were employed within the LCAO simulations regardless of the Hamiltonian adopted.

For pure BLYP we found that the lattice parameters obtained by the LCAO method are in slightly better agreement with experimental values when compared with those obtained using the PW approach (see Table 1). The explanation is that the Fe–Fe distances (sFe–Fe and lFe–Fe) are slightly longer in the PW calculations, while the Fe–O distances are similar for both methods (see Table 1).

To our knowledge, no one has focused on how the choice of U or Hartree–Fock exchange affects the geometrical structure of this particular Fe-oxide. A first glance of Table 1 lets us understand that the BLYP + U approach (for several values of the U) causes an elongation of both the lFe–Fe and Fe–O distances when the U-value gets larger, even though the sFe–Fe distance decreases (see Fig. 2).

Consequently, the lattice parameters get bigger with increasing U-value. This is furthermore highlighted looking at the volume of the rhombohedral cell (see Fig. 3).

In fact, by increasing the U-value the volume of the cell expands away from the value reported experimentally. This observation is explained by the increasing repulsion on the Fe-sites as the U-value increases (see Table 1 and Fig. 3), and has also been reported for DFT + U calculations on, for example, α-Cr_2O_3.[11]

The hybrid-functionals show the opposite behaviour. As the HF exchange value increases to 50% the volume decreases to match the experimental one (see Fig. 3 and Table 1). This is also reflected in the bond distances which are decreasing with higher HF exchange (Fig. 2 and Table 1).

We conclude that of the methods discussed the F50LYP functional is the most suitable in describing the geometrical

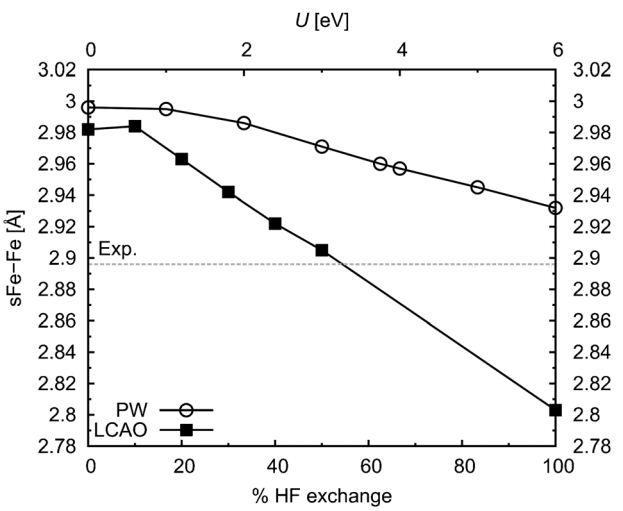

Fig. 2 BLYP sFe–Fe bond length (see Fe1–Fe2 in Fig. 1) *vs.* several values of the U and percentage of HF. Bond lengths are expressed in Å, while U in eV.

View Article Online

Published on 15 June 2011. Downloaded by National University of Singapore on 12/2/2018 5:54:21 AM.

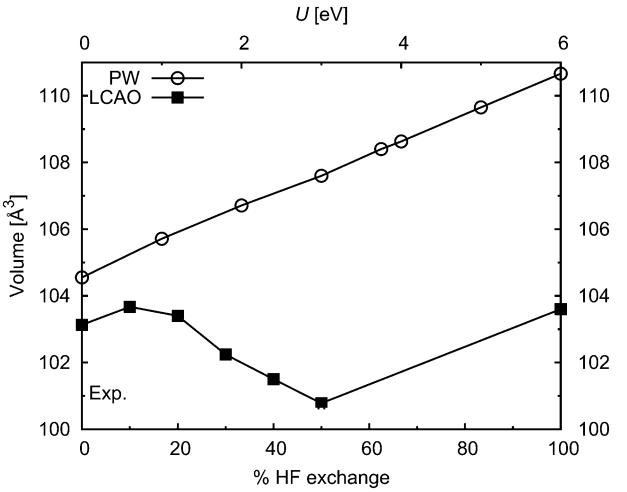

Fig. 3 BLYP volume of rhombohedral α-Fe_2O_3 as a function of different percentages of HF exchange and U. Volume is in Å^3, U in eV.

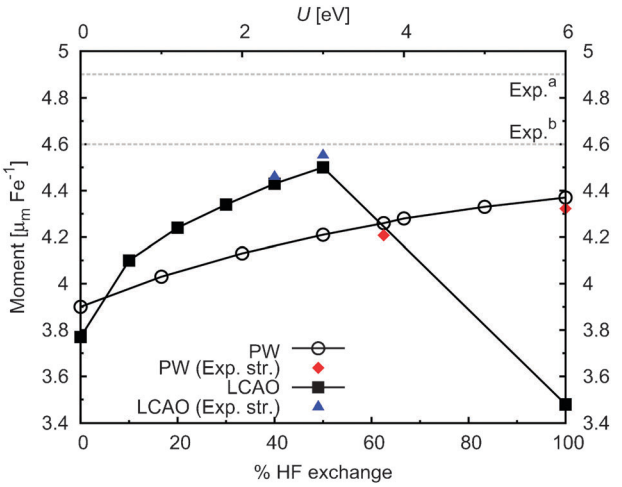

Fig. 4 BLYP magnetic moment of the rhombohedral α-Fe_2O_3 as a function of different percentages of HF exchange and U compared with the experimental values 4.9 μ_m/Fe (Exp.[a])[74] and 4.6μ_m/Fe (Exp.[b]),[74] respectively. μ_m magnetic moment in μ_m/Fe and U in eV. Red rhombus and blue triangles represent the magnetic moments calculated by using the experimental structure with LCAO and PW approaches, respectively.

features of α-Fe_2O_3. Whereas, the BLYP + U approach seems to overestimate volume and bond distances, especially for higher values of U.

3.2 Magnetic properties

The magnetic moment (μ_m) like the structural parameters analysed above highly depends on the behavior of the electronic structure. In the PW framework magnetic moments were extracted from the projected density of states through the Lödwing decomposition of charges on angular momentum and spin components of iron atoms.[55] Analogously, for the LCAO calculations Mulliken charges and spin analysis were employed to evaluate the magnetic moments.[56]

The dependence of the magnetic moment on U and the values of HF percentage is depicted in Fig. 4.

By looking at the PW and LCAO graph (see Fig. 4), it is predicted that BLYP underestimates the experimental data. By increasing the values of U or HF exchange the magnetic moment increases, however, the experimental value is still not matched for U = 6 eV (see Fig. 4). The increase of the magnetic moments when the HF contribution and U-value are introduced is mainly due to the improved localisation of the d electrons. However, also electron correlation contributes to the magnetic description, which is highlighted by the low μ_m-value for the pure HF simulation (see Fig. 4). Such an effect has already been observed for similar strong-correlated materials.[14]

Once again the 50% of HF exchange approaches the experimental values (see Fig. 4),[74] but the magnetic moment is still underestimated by about 0.4 μ_m (*ca.* 8%) or 0.1 μ_m (*ca.* 0.2%) when compared with the two different experimental values of 4.9 μ_m and 4.6 μ_m, respectively (see Fig. 4).

As the magnetic moment is structure dependent, we also calculated μ_m using the experimental structure for the F40LYP and F50LYP functionals, as well as U = 3.75 and 6 eV. All these values are similar to those obtained after optimisation, *i.e.* μ_m are 4.5, 4.6, 4.2 and 4.3 μ_m/Fe for the F40LYP, F50LYP and BLYP + U (U = 3.75 and 6 eV), respectively.

3.3 Electronic structure

As remarked before, α-Fe_2O_3 is experimentally reported to be a charge-transfer insulator, but traditional LDA and GGA functionals describe it as a Mott insulator. This can be rectified by employing DFT + U or hybrid-functionals. Here we compare these approaches to understand the difference in the electronic structures.

Firstly, we determined the direct (at the Γ point) energy band gap (EBG) of the fully optimized α-Fe_2O_3 for several values of U, spanning between 0 (pure BLYP) and 6 eV, and for different Hartree–Fock exchange percentages between 0% and 100%. We also measured the EBG for the optimized value of the U, 3.75 eV. Fig. 5(a) and (b) show the trends of the hematite energy band gap when the U value or the HF percentage are varied.

To make sure that our calculations were reliable we also employed the PBE functional. Fig. 5 shows that for pure BLYP, both the PW and LCAO approaches underestimate the energy band gap of hematite. The pure BLYP and even PBE band gaps are in the same region (see Fig. 5).

From Fig. 5 it can also be seen that the EBG is not matched even for very high values of U (5, 6 eV), while most hybrid-functionals instead overestimate the EBG when compared to the experimental value of 2.0 eV.[22] It is well known that pure HF overestimates the EBG due to the over-localization of the 3d electrons on the iron atoms.[23] The energy band gap agrees only with the experimental value for low percentage values of HF exchange (*i.e.* 9.6%). This behaviour is recognised for most hybrid-functionals and depends on the long-range self-interaction problem discussed for example by Handy, Scuseria and co-workers.[7,33–35,75–78] The hybrid-functionals HSE derived by Heyd and co-workers correct for this weakness as discussed in the Introduction section.[75,78]

 This journal is © the Owner Societies 2011

View Article Online

Published on 15 June 2011. Downloaded by National University of Singapore on 12/2/2018 5:54:21 AM.

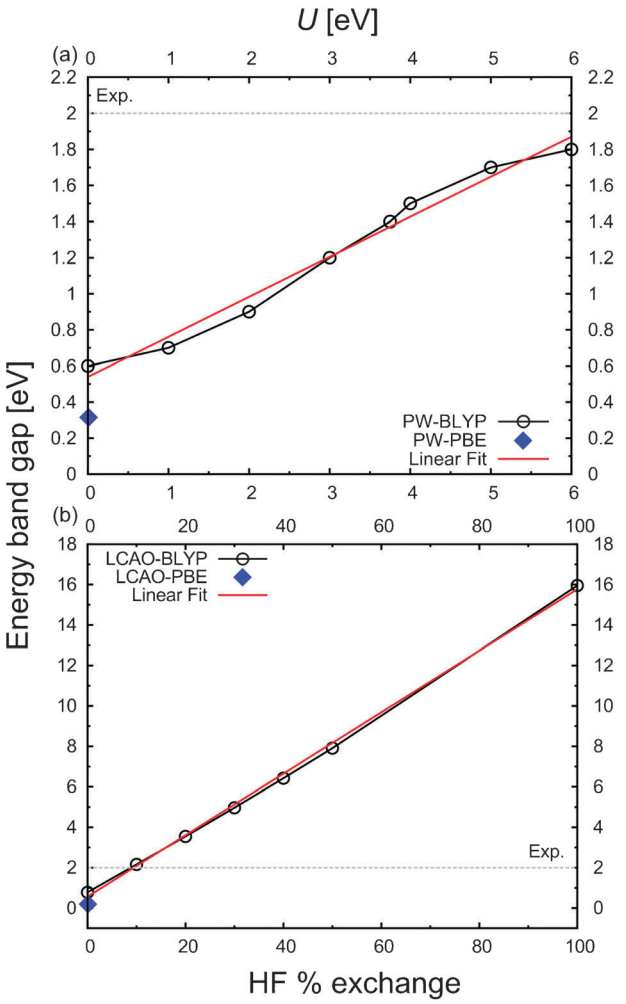

Fig. 5 In (a) and (b) the energy band gap as a function of the *U*-value and the HF percentages are shown, respectively. *U* in eV.

To determine the electronic character of α-Fe_2O_3, the density of states (DOS) along with its projection on the atomic orbitals (pDOS) are presented in Fig. 6.

Here, we compare the total and partial DOS of hematite gathered for the most relevant cases in the PW and LCAO frameworks.

DOS and pDOS carried out with pure BLYP are shown in Fig. 6(a) and (b) for the PW and LCAO methods, respectively. These two profiles are very similar, both methods show a broad band in the range −2 to −8 eV described by an hybridization between the Fe(3d) and O(2sp) states. As a result the valence-band edge is Fe(3d) dominated, when it should have been characterised by O(2p), proposing a band gap transition from a Fe(3d) to a Fe(3d) state. Hematite is then wrongly predicted as a Mott insulator with the BLYP functional.

Fig. 6(c) and (d) report DOS and pDOS of hematite for BLYP + *U* (*U* = 2 eV) and B3LYP, respectively. The first observation regarding these models is that the Fe(3d) electrons, which were highly delocalised in the BLYP simulations, appear to localise, and are seen as peaks around −6 eV. The highest occupied states in the VB (zone just below 0 eV), involved in the band gap transition, still appear as a hybridisation of Fe(3d) and O(2sp) orbitals. This means that 2 eV for DFT + *U* and 20% of HF exchange (B3LYP) are not sufficient to describe α-Fe_2O_3 as a charge-transfer insulator.

In the end, Fig. 6(e) and (f) report the total and projected DOS of hematite for BLYP + *U* (*U* = 3.75 eV) (where the value of *U* has been optimized) and F40LYP, respectively. The valence bands are predominated by the presence of the O(2sp) states and the band gap transition turns out to be correct (from a O(2sp) to a Fe(3d) state). In fact, the region described by localised Fe(3d) states, between *ca.* −6 and −8 eV in Fig. 6(e) and (f), is now well separated from the valence bands. Similar behaviour is found for BLYP + *U* (*U* = 6 eV, see Fig. 6(h)). Noteworthy is the similarity between the DOS profiles evaluated with F40LYP where Fe atoms are described both by means of an all-electron basis-set and an ECP, respectively (see Fig. 6(f) and (h)). Hence, the pseudo-potential description is not altering the nature of the charge-transfer character of hematite.

We now move our attention to the behavior of the conduction band. Regardless of the computational method, the CB is typically described by the spin-down Fe(3d) states depicted in most of the cases as two distinct bands (see Fig. 6).

XANES spectroscopy is a powerful technique which provides information about the conduction bands in solids.[24,79–82] Previous XANES studies on the Fe K-edge in α-Fe_2O_3 have identified that most of the pre-edge absorption involves the Fe(3d) states.[24,80,81] XANES data, collected by us, for the Fe K-edge, in α-Fe_2O_3, are presented in Fig. 7.

The features A and B, in the spectrum, are assigned to the Fe(3d) spin-down electrons in the conduction bands of α-Fe_2O_3, while peak C, broader than A and B, is described by the Fe(3d) spin-up electrons.[24,80,81] Glatzel *et al.* also demonstrated how peaks A and B have some p character, coming from the hybridization of Fe(3d) with O(2p) in the close vicinity.[24]

The Fe(3d) spin-down conduction bands of the pure BLYP methods, shown in Fig. 6(a) and (b), are superimposed on the experimental XANES spectrum in Fig. 7. Experimentally the peak denoted A should have a lower intensity than peak B. The BLYP method instead predicts the A peak to be more intense than B.

Unfortunately, by increasing the magnitude of the *U* the intensity of peak A increases further, whereas the band above (B) decreases in intensity (see Fig. 6(a), (c) and (e)), failing to correctly mimic the experimental XANES spectrum. This includes the BLYP + *U* simulation using the optimised *U*-value of 3.75 eV (see Fig. 6(e) and 7). In fact the correct intensity order, for BLYP + *U* is only recovered when using *U*-values $\geq$ 6 (see Fig. 6(g) and 7).

Varying the percentage of the Hartree–Fock exchange has a different effect on the intensities of the Fe(3d) pDOS in the conduction band: increasing the HF-exchange shows a decrease in intensity of the peak A (see Fig. 7). When the percentage of the HF exchange is lifted to 40% (F40LYP) the order of the intensities switches abruptly, agreeing with the order of intensities of the experimental peaks A and B (see Fig. 7). It is worth noting that the B3LYP functional, in this study, fails to predict the experimental XANES spectrum.

View Article Online

Published on 15 June 2011. Downloaded by National University of Singapore on 12/2/2018 5:54:21 AM.

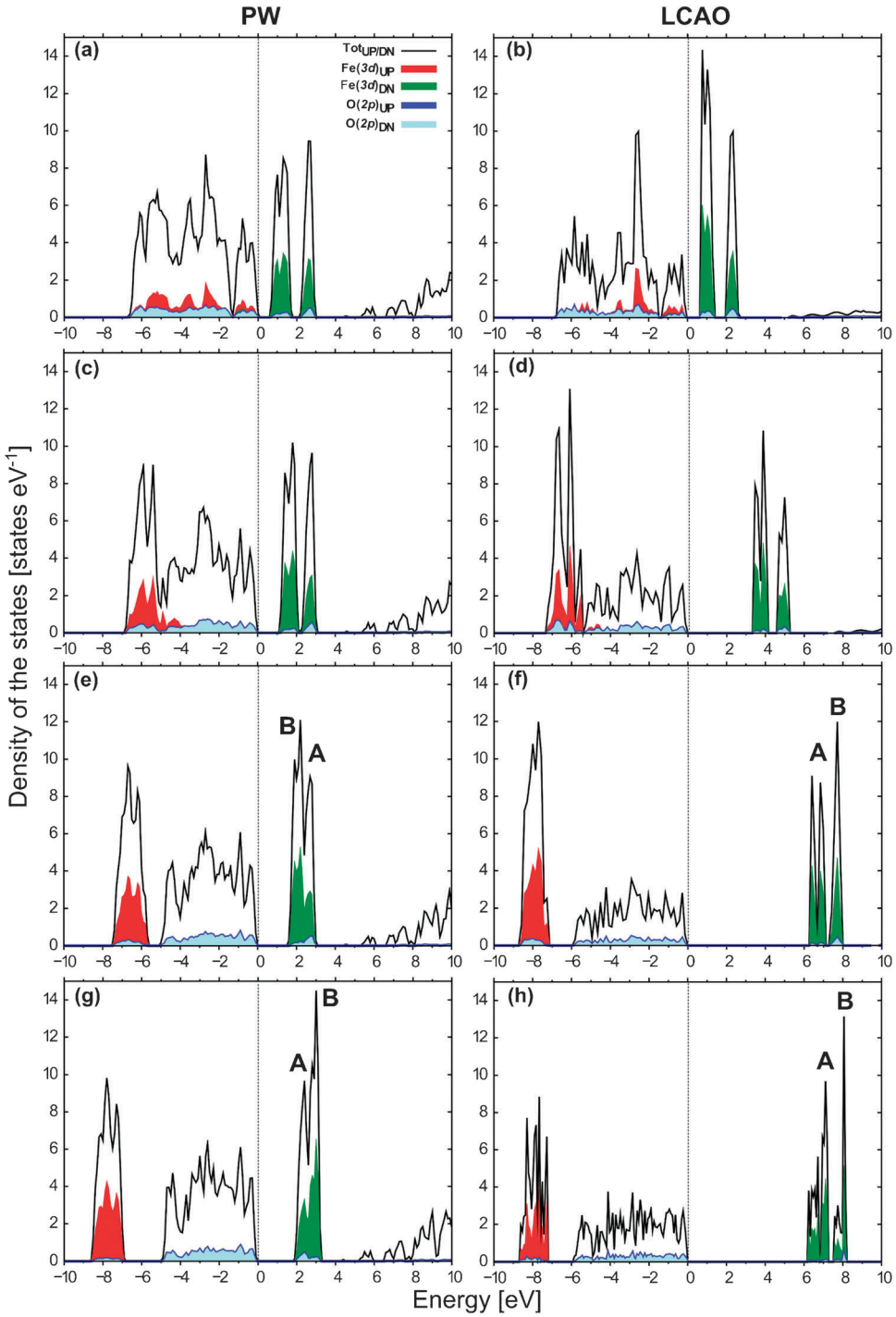

Fig. 6 Total and projected DOS of the full optimized α-Fe_2O_3: (a) pure BLYP PWscf, (b) pure BLYP CRYSTAL06, (c) BLYP + 2 eV, (d) B3LYP, (e) BLYP + 3.75, (f) F40LYP, (g) BLYP + 6 eV and (h) F40LYP with ECP. Assignments of A and B in (e), (f) and (g) are described in Fig. 7. Black lines for total DOS, red and green lines for Fe(3d) up and down, respectively, whereas blue and light-blue for O(2p) up and down respectively.

The intensities of peaks A and B are related to the symmetry of the orbitals dominating the bands. Hence, an accurate symmetry classification on how Fe(3d) orbitals are split in the octahedral electric field, exerted by the oxygens, assigned peaks A and B to t_g and e orbitals respectively.[24] The classification by symmetry of the Fe(3d) (spin-down) orbitals, obtained with F40LYP, matches the experimental assignation (see Fig. 6) demonstrating that the Fe(3d) t_g orbitals fall at lower energies than e ones. Such a behaviour is kept when varying the HF percentage. On the other hand, our DFT and DFT + U simulations,[13,18] within the PW approximation, propose the wrong symmetry-splitting of the Fe(3d) orbitals, putting the e at lower energies. Only for U = 6 eV (or eventually higher) the t_g orbitals are dominating the lowest CB states, as seen in Fig. 6(g).

 This journal is © the Owner Societies 2011

View Article Online

Published on 15 June 2011. Downloaded by National University of Singapore on 12/2/2018 5:54:21 AM.

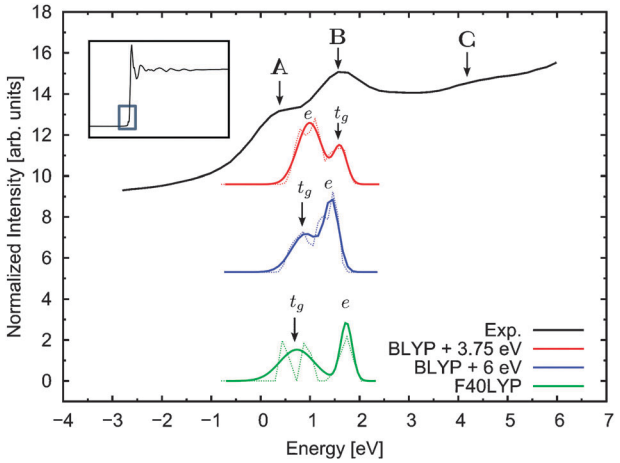

Fig. 7 Comparison of the experimental XANES Fe K-edge spectrum of α-Fe_2O_3 and the spin-down pDOS obtained with BLYP + 3.75 eV, BLYP + 6 eV and F40LYP. The pDOSs (thin dashed lines) were fitted with Gaussian functions (thick solid lines). Intensities are in arbitrary units, while energy in eV. pDOS were shifted to 0 eV. The XANES spectrum was also shifted at lower energy to fit the theoretical pDOSs. The inset shows the entire EXAFS (extended X-ray absorption fine structure) spectrum in which is highlighted the area corresponding to the XANES in the comparison.

Peak C shown in Fig. 7 is a mixture of Fe(3d) spin-up and spin-down orbitals in agreement with previous analysis by Glatzel *et al.*[24] Note this feature is not described in Fig. 6.

Regarding the partial 2p character of the conduction band in hematite, we found that the Fe(3d) states hybridize with a small amount of O(2sp) states as seen in the DOS profiles in Fig. 6. This agrees with what has been found by Glatzel *et al.*[24] However, this does not depend on the amount of U or HF exchange introduced in the BLYP.

D. Conclusions and discussion

The electronic, the geometrical and the magnetic properties of the corundum-type α-Fe_2O_3 have been determined and compared within the PW and the LCAO frameworks. To deal with the self-interaction error in this strongly correlated material we used two approaches: (1) Hubbard correction (DFT + U) and (2) hybrid-BLYP. We optimized, in a self-consistent way, the appropriate value of the U (3.75 eV), as well as varying the U-value and the percentage of HF exchange in an empirical manner to obtain properties in agreement with experimental data.

By employing these approaches we have shown that:

■ α-Fe_2O_3 is correctly described as a charge-transfer insulator, when the optimized value for the U (3.75 eV) or the 40% of HF exchange is employed.

■ The popular B3LYP functional fails in describing α-Fe_2O_3 as a charge-transfer insulator. Instead B3LYP predicts α-Fe_2O_3 as a Mott insulator, in agreement with pure DFT functionals, such as BLYP. Similar weaknesses of the B3LYP functional have been discussed previously in the literature.[7,10,71,83] It has been proposed that strongly correlated solids, such as iron oxides, require at least 30% sometimes up to 50% of Hartree–Fock exchange to work out the correct electronic structure.[71]

The latter conclusion is further sustained when the order of the intensities and symmetries of the Fe(3d) pDOS, in the conduction band, of the hematite is compared with the experimental Fe K-edge XANES spectrum. We observe that:

■ For the hybrid functionals the experimental intensities were reproduced only by employing 40% of Hartree–Fock exchange combined with the BLYP functional.

■ The correct symmetry classification of the Fe(3d) orbitals in the conduction band was obtained for all simulations carried out within the LCAO approximation.

■ Only for U-values larger than 6 eV the correct classification of the conduction band is reported.

To summarise we find that geometrical structure, magnetic and electronic features of hematite are reproduced by F40LYP. Regarding BLYP + U, no single U-value reproduces all properties satisfactorily. Instead it is found that the geometrical structure is best addressed by using pure BLYP, as the Columbic repulsion increases the volume when U is introduced. On the other hand, the electronic description of the valence and conduction bands is only accounted for by $U \geq 6$ eV. Hence, to predict and interpret XANES spectra for more complex iron oxide materials, using a single Hamiltonian technique, both F40LYP and BLYP + U ($U \geq 6$ eV) can be employed.

Finally, we want to emphasize that the optimal value of the U and the HF percentage are very crucial in the study of hematite and depend on what properties need to be studied, but the choice between DFT + U or hybrid-functional techniques to treat strongly correlated systems must be left to the investigator.

Acknowledgements

This research was supported by a UKC Scholarship from University of Kent. The authors wish to acknowledge Matteo Cococcioni at University of Minnesota for the useful suggestions concerning the optimization of the U with PWscf. We are grateful to the NIS Center of Excellence at University of Turin (Italy) for having provided part of the computer time requested to carry out these results. The authors would like to acknowledge the use of the UK National Grid Service in carrying out this work. We also acknowledge SOLEIL (GIF-sur-YVETTE, Paris) for provision of synchrotron radiation facilities and we would like to thank Stéphanie Belin for assistance in using beamline SAMBA.

Notes and references

1 W. Kohn and L. J. Sham, *Phys. Rev.*, 1965, **140**, 1133–1138.
2 P. Hohenberg and W. Kohn, *Phys. Rev.*, 1964, **136**, 864–871.
3 Z. Wei-Bing, H. Yu-Lin, H. Ke-Li and T. Bi-Yu, *J. Phys.: Condens. Matter*, 2006, **18**, 9691–9701.
4 M. Marsman, J. Paier, A. Stroppa and G. Kresse, *J. Phys.: Condens. Matter*, 2008, **20**, 064201.
5 F. Tran, P. Blaha, K. Schwarz and P. Novak, *Phys. Rev. B: Condens. Matter Mater. Phys.*, 2006, **74**, 155108–155110.
6 I. P. R. Moreira, F. Illas and R. L. Martin, *Phys. Rev. B: Condens. Matter*, 2002, **65**, 155102–155114.
7 P. Rivero, I. P. R. Moreira, G. E. Scuseria and F. Illas, *Phys. Rev. B: Condens. Matter Mater. Phys.*, 2009, **79**, 245129–245129.
8 T. Bredow and A. R. Gerson, *Phys. Rev. B: Condens. Matter*, 2000, **61**, 5194–5201.

View Article Online

Published on 15 June 2011. Downloaded by National University of Singapore on 12/2/2018 5:54:21 AM.

9 C. Franchini, R. Podloucky, J. Paier, M. Marsman and G. Kresse, *Phys. Rev. B: Condens. Matter Mater. Phys.*, 2007, **75**, 195128–195111.
10 M. Alfredsson, D. G. Price, C. R. A. Catlow, S. C. Parker, R. Orlando and J. P. Brodholt, *Phys. Rev. B: Condens. Matter Mater. Phys.*, 2004, **70**, 165111–165116.
11 N. J. Mosey and E. A. Carter, *Phys. Rev. B: Condens. Matter Mater. Phys.*, 2007, **76**, 155123–155113.
12 N. C. Wilson and S. P. Russo, *Phys. Rev. B: Condens. Matter*, 2009, **79**, 0941131–0941113.
13 G. Rollmann, A. Rohrbach, P. Entel and J. Hafneer, *Phys. Rev. B: Condens. Matter Mater. Phys.*, 2004, **69**, 16510701–16510712.
14 X. Feng and N. M. Harrison, *Phys. Rev. B: Condens. Matter Mater. Phys.*, 2004, **70**, 092402–092404.
15 M. Cococcioni and S. de Gironcoli, *Phys. Rev. B: Condens. Matter Mater. Phys.*, 2005, **71**, 035105–035116.
16 H. J. Kulik, M. Cococcioni, D. A. Scherlis and N. Marzari, *Phys. Rev. Lett.*, 2006, **97**, 103001–103004.
17 M. Catti, G. Valerio and R. Dovesi, *Phys. Rev. B: Condens. Matter*, 1995, **51**, 7441–7450.
18 M. Blanchard, M. Lazzeri, F. Mauri and E. Balan, *Am. Mineral.*, 2008, **93**, 1019–1027.
19 M. P. J. Punkkinen, K. Kokko, W. Hergert and I. J. Väyrynen, *J. Phys.: Condens. Matter*, 1999, **11**, 2341–2349.
20 Y. Xu, T. Boonfueng, L. Axe, S. Maeng and T. Tyson, *J. Colloid Interface Sci.*, 2006, **299**, 28–40.
21 S. E. Manson, C. R. Iceman, K. S. Tanwar, T. P. Trainor and A. M. Chaka, *J. Phys. Chem. C*, 2009, **113**, 2159–2170.
22 L. W. Finger and R. M. Hazen, *J. Appl. Phys.*, 1980, **51**, 5362–5367.
23 M. Catti and G. Sandrone, *Faraday Discuss.*, 1997, **106**, 189–203.
24 P. Glatzel, A. Mirone, S. G. Eeckhout, M. Sikora and G. Giuli, *Phys. Rev. B: Condens. Matter Mater. Phys.*, 2008, **77**, 115133.
25 F. Aquilante, P.-A. Malmqvist, T. B. Pedersen, A. G. Ghosh and B. O. Roos, *J. Chem. Theory Comput.*, 2008, **4**, 694–702.
26 J.-W. Song, S. Tokura, T. Sato, M. A. Watson and K. Hirao, *J. Chem. Phys.*, 2007, **127**, 154109–154114.
27 M. A. Rohrdanz, K. M. Martins and J. M. Herbert, *J. Chem. Phys.*, 2009, **130**, 054112.
28 Y. Tawada, T. Tsuneda, S. Yanagisawa, T. Yanai and K. Hirao, *J. Chem. Phys.*, 2004, **120**, 8425–8433.
29 R. Kishi, S. Bonness, K. Yoneda, H. Takahashi, M. Nakano, E. Botek, B. Champagne, T. Kubo, K. Kamada, K. Ohta and T. Tsuneda, *J. Chem. Phys.*, 2010, **132**, 094107–094111.
30 G. Mazur, M. Makowski, R. Włodarczyk and Y. Aoki, *Int. J. Quantum Chem.*, 2011, **111**, 819–825.
31 A. G. Eguiluz, O. D. Restrepo, B. C. Larson, J. Z. Tischler, P. Zschack and G. E. Jellison, *J. Phys. Chem. Solids*, 2005, **66**, 2281–2289.
32 T. Ziegler, M. Seth, M. Krykunov, J. Autschbach and F. Wang, *THEOCHEM*, 2009, **914**, 106–109.
33 K. Hummer, J. Harl and G. Kresse, *Phys. Rev. B: Condens. Matter Mater. Phys.*, 2009, **80**, 115205.
34 I. S. Lim and G. E. Scuseria, *Chem. Phys. Lett.*, 2008, **460**, 137–140.
35 J. Uddin and G. E. Scuseria, *Phys. Rev. B: Condens. Matter Mater. Phys.*, 2005, **72**, 035101.
36 K. Otsuka, T. Kaburagi, C. Yamada and S. Takenaka, *J. Power Sources*, 2003, **122**, 111–121.
37 V. Hacker, R. Vallant and M. Thaler, *Ind. Eng. Chem. Res.*, 2007, **46**, 189–192.
38 H. Imanishi and A. Maeda, *Int. J. Chem. React. Eng.*, 2007, **5**, A109.
39 U. Becker, M. F. Hochella Jr and E. Apra', *Am. Mineral.*, 1996, **81**, 1301–1314.
40 E. Liger, L. Charlet and P. Van Cappellen, *Geochim. Cosmochim. Acta*, 1999, **63**, 2939–2955.
41 W. Zhang, J. Chen, X. Wang, H. L. Qi and K. S. Peng, *Appl. Organomet. Chem.*, 2009, **23**, 200–203.
42 J. G. Catalano, C. Park, P. Fenter and Z. Zhang, *Geochim. Cosmochim. Acta*, 2008, **72**, 1986–2004.
43 J. C. Catalano, P. Fenter and C. Park, *Geochim. Cosmochim. Acta*, 2009, **73**, 2242–2251.
44 S. E. O'Reilly and M. F. Hochella Jr., *Geochim. Cosmochim. Acta*, 2003, **67**(23), 4471–4487.
45 C. Liu and P. M. Huang, *Geochim. Cosmochim. Acta*, 2003, **67**(5), 1045–1054.
46 P. Robinson, R. J. Harrison, S. A. McEnroe and R. B. Hargraves, *Am. Mineral.*, 2004, **89**, 725–747.
47 E. F. Covelo, F. A. Vega and M. L. Andrade, *J. Hazard. Mater.*, 2007, **140**, 308–315.
48 G. Magnacca, G. Cerrato, C. Morterra, M. Signoretto, F. Somma and F. Pinna, *Chem. Mater.*, 2003, **15**, 675–687.
49 Y. Joseph, M. Wuhn, A. Niklewski, W. Ranke, W. Weiss, C. Woll and R. Schlogl, *Phys. Chem. Chem. Phys.*, 2000, **2**, 5314–5319.
50 J. W. Sun, D. K. Zhong and D. R. Gamelin, *Energy Environ. Sci.*, 2010, **3**, 1252–1261.
51 D. K. Zhong, J. W. Sun, H. Inumaru and D. R. Gamelin, *J. Am. Chem. Soc.*, 2009, **131**, 6086–6087.
52 A. Kay, I. Cesar and M. Gratzel, *J. Am. Chem. Soc.*, 2006, **128**, 15714–15721.
53 J. Brillet, M. Gratzel and K. Sivula, *Nano Lett.*, 2010, **10**, 4155–4160.
54 R. Z. Blacke, R. E. Hessevick, T. Zoltai and L. W. Finger, *Am. Mineral.*, 1966, **51**, 123–129.
55 S. Baroni, A. Dal Corso, S. de Gironcoli, P. Giannozzi, C. Cavazzoni, G. Ballabio, S. Scandolo, G. Chiarotti, P. Focher, A. Pasquarello, K. Laasonen, A. Trave, R. Car, N. Marzari and A. Kokalj, *PWscf*, 2006.
56 R. Dovesi, V. R. Saunders, C. Roetti, R. Orlando, C. M. Zicovich-Wilson, F. Pascale, B. Civalleri, K. Doll, N. M. Harrison, I. J. Bush, P. D'Arco and M. Llunell, *CRYSTAL 06, User Manual*, 2006.
57 D. Vanderbilt, *Phys. Rev. B: Condens. Matter*, 1990, **41**, 7892–7895.
58 A. D. Becke, *Phys. Rev. A: At., Mol., Opt. Phys.*, 1988, **38**, 3098–3100.
59 C. Lee, W. Yang and R. G. Parr, *Phys. Rev. B*, 1988, **37**, 785–789.
60 J. P. Perdew, B. Burke and M. Ernzerhof, *Phys. Rev. Lett.*, 1996, **77**, 3865–3868.
61 C. G. Broyden, *SIAM J. Appl. Math*, 1970, **6**, 76–90.
62 R. Fletcher, *Comput. J.*, 1970, **J13**, 317–322.
63 D. Goldfarb, *Math. Comput. Modell.*, 1970, **24**, 23–26.
64 D. F. Shanno, *Math. Comput. Modell.*, 1970, **24**, 647–656.
65 V. I. Anisimov, F. Aryasetiawan and A. I. Lichtenstein, *J. Phys.: Condens. Matter*, 1997, **9**, 767–808.
66 M. I. McCarthy and N. M. Harrison, *Phys. Rev. B: Condens. Matter*, 1994, **49**, 8574–8582.
67 J. S. Binkley, J. A. Pople and W. J. Hehre, *J. Am. Chem. Soc.*, 1980, **102**, 939–947.
68 W. J. Stevens, H. Basch and M. Krauss, *J. Chem. Phys.*, 1984, **81**, 6026–6033.
69 W. J. Stevens, M. Krauss, H. Basch and P. G. Jasien, *Can. J. Chem.*, 1992, **70**, 612–630.
70 W. Koch and M. C. Holthausen, *A Chemist's Guide to Density Functional Theory*, Wiley-VCH Verlag GmbH, Weinheim, 2nd edn, 2001.
71 F. Cora', M. Alfredsson, G. Mallia, D. S. Middlemiss, W. C. Mackrodt, R. Dovesi and R. Orlando, *Principles and Applications of Density Functional Theory in Inorganic Chemistry II, Structure and Bonding*, ed. N. Kaltsoyannis and J. E. McGrady, Springer-Verlag Berlin, 2004, vol. 113, pp. 171–232.
72 A. D. Becke, *J. Chem. Phys.*, 1993, **98**, 5648–5652.
73 S. M. Webb, *Phys. Scr., T*, 2005, **115**, 1011–1014.
74 J. M. D. Coey and G. A. Sawatzky, *J. Phys. C: Solid State Phys.*, 1971, **4**, 2386.
75 J. Heyd, G. E. Scuseria and M. Ernzerhof, *J. Chem. Phys.*, 2003, **118**, 8207–8215.
76 D. J. Tozer, R. D. Amos, N. C. Handy, B. O. Roos and L. Serrano-Andres, *Mol. Phys.*, 1999, **97**, 859–868.
77 T. Yanai, D. P. Tew and N. C. Handy, *Chem. Phys. Lett.*, 2004, **393**, 51–57.
78 J. Heyd, G. E. Scuseria and M. Ernzerhof, *J. Chem. Phys.*, 2006, **124**, 219906.
79 B. Gilbert, C. Frandsen, E. R. Maxey and D. M. Sherman, *Phys. Rev. B: Condens. Matter*, 2009, **79**, 035108–035107.
80 H. Modrow, S. Bucher, J. J. Rehr and A. L. Ankudinov, *Phys. Rev. B: Condens. Matter*, 2003, **67**, 035123–035110.
81 L. X. Chen, T. Liu, M. C. Thurnauer, R. Csencsits and T. Rajh, *J. Phys. Chem. B*, 2002, **106**, 8539–8546.
82 M. Pollak, M. Gautier, N. Thromat, S. Gota, W. C. Mackrodt and V. R. Saunders, *Nucl. Instrum. Methods Phys. Res., Sect. B*, 1995, **97**, 383–386.
83 J. Paier, M. Marsman and G. Kresse, *J. Chem. Phys.*, 2007, **127**, 024103–024110.

 This journal is © the Owner Societies 2011